Numerical Determination of Induced Electric Eddy Fields Inside Arbitrarily Shaped Induction Coils

IEPC-2013-85

Presented at the 33^{rd} International Electric Propulsion Conference,
The George Washington University, Washington, D.C., USA
October 6–10, 2013

Chris Volkmar*, Jens Simon†, and Ubbo Ricklefs‡
Technische Hochschule Mittelhessen University of Applied Sciences, 35390 Giessen, Germany

Abstract: We propose a numerical solution of Faraday's law of induction based on the knowledge of the time-varying, non-uniform vector potential inside arbitrarily shaped electrical coils. The vector potential can be related to the magnetic induction which yields the well known form of Faraday's law. The algorithm applies for non-retarding fields within the quasi-stationary regime.

The model is intended to help to understand the behavior of electromagnetic fields inside the discharge chambers of radio-frequency ion thrusters. This knowledge of the electromagnetic field distribution provides a basis for modeling an inductively-coupled plasma which is kept burning by absorbing electromagnetic energy. In the long run, this plasma model will be used to support development processes of electric and electronic control devices which are needed for driving radio-frequency ion thrusters more efficiently.

To predict the induced radio frequency fields more precisely, the skin effect along the coil wire is modeled. Furthermore, an impedance model of the coil, which incorporates the skin effect, is introduced.

The simulated data are compared to measured values obtained by a generic electric field probe. Although the probe was uncalibrated, the observed values were highly similar to the expected values as determined by the numerical solution.

Nomenclature

$\mathbf{A}$	= Vector potential vector ($\mathrm{V\,s\,m^{-1}}$)	t	= Time (s)
A_{eff}	= Effective coil area ($\mathrm{m^2}$)	$v\,(t)$	= Radio-frequency voltage (V)
$\mathbf{B}$	= Magnetic induction vector (T)	$\hat{v}$	= Radio-frequency voltage amplitude (V)
B	= Magnetic induction field strength (T)	v_{e}	= Effective exhaust velocity ($\mathrm{m\,s^{-1}}$)
c_0	= Speed of light in vacuum ($\mathrm{m\,s^{-1}}$)	$\mathbf{x}$	= Cartesian vector to sampling points (m)
$\mathbf{E}$	= Electric field vector ($\mathrm{V\,m^{-1}}$)	$\mathbf{x}'$	= Cartesian vector to coil elements (m)
E	= Electric field strength ($\mathrm{V\,m^{-1}}$)	Z	= Coil impedance (Ω)
f	= Frequency (Hz)	δ	= Skin depth (m)
g_0	= Gravitational acceleration ($\mathrm{m\,s^{-2}}$)	Φ	= Scalar potential (V)
$\mathbf{H}$	= Magnetic field vector ($\mathrm{A\,m^{-1}}$)	λ	= Wavelength (m)
I_{sp}	= Specific impulse (s)	μ_0	= Vacuum permeability ($\mathrm{Wb\,A^{-1}\,m^{-1}}$)
$\mathbf{J}$	= Current density vector ($\mathrm{A\,m^{-2}}$)	μ_{r}	= Relative permeability (dimensionless)
L	= Coil inductance (H)	σ	= Conductivity ($\mathrm{S\,m^{-1}}$)
l	= Coil length (m)	ω	= Angular frequency ($\mathrm{s^{-1}}$)

*Research Scientist, Department of Electrical Engineering, chris.volkmar@ei.thm.de
†Research Scientist, Department of Electrical Engineering, jens.simon@ei.thm.de
‡Professor, Department of Electrical Engineering, ubbo.ricklefs@ei.thm.de

I. Introduction

Over the past 20 years, the importance of electrostatic thrusters, such as radio-frequency ion thrusters (RITs), has been steadily increasing. Electric propulsion systems based on RIT technology not only play a major role in space applications, but also in terrestrial applications like materials processing.[1] That is primarily due to their energy efficiency, scalability, and purity of the plasma based on the electrodeless discharge.

Compared to chemical propulsion systems, RITs offer thrusts with very high specific impulses $I_{\mathrm{sp}} = v_{\mathrm{e}}/g_0$; i.e., very high exhaust velocities of the thrust-generating ions. Additionally, their limited demand for fuel allows space missions to be designed to last many years.[2,3] Despite these advantages, the ignition process still offers room for further improvement in terms of energy and gas consumption.

Together with Giessen University—alma mater of Horst Loeb, who invented RITs in the 1960s[4]—our research group works on optimizing the thrusters' overall efficiency by developing peripheral devices such as matching circuits and control loops. This requires a description of the system from an engineering point of view. To obtain an equivalent circuit diagram of the thruster which includes the electrical parameters needed for the design of any kind of peripheral device, the core of the thruster—the inductively-coupled plasma—has to be fully understood and modeled. This is still part of the ongoing work.

In this paper, we introduce a numerical solver for Faraday's Law of induction in its differential form, given by

$$\nabla \times \mathbf{E} = -\frac{\partial \mathbf{B}}{\partial t}. \tag{1}$$

The magnetic induction inside a vacuum filled vessel within a Cartesian simulation domain was obtained with a static magnetic field solver, details are given elsewhere.[5] These data were used to determine the self-inductance for arbitrary coil geometries which is an important parameter for the design of matching networks used to optimize the ignition process for inductively-coupled plasmas (ICP). It also offers the opportunity to easily simulate induced electric eddy fields if a time dependence of the magnetic induction—and hence of the vector potential—is assumed.

The next sections give background of the theories used, their algorithmic adaption, simulated results, and the verification of the resulting data with probe measurements.

II. Theory and Algorithmic Adaptation

The goal of the developed solver is the description of the coupled, self-consistent electromagnetic fields inside a radio-frequency (rf) driven electrical coil. As the applied frequencies lie in the lower MHz-range, wave propagation does not have to be taken into account. The typical wire length for ICP coils is below 2 m, which is only a fraction of the wavelength of the applied rf signals, according to $\lambda = c_0/f$. If this constraint applies, the rf current through the coil can be assumed homogeneous and the governing equations from the quasi-stationary regime can be used for calculus.[5,6] Furthermore, coils that match this constraint are said to be electrically short.

A. Theoretical Background

In a preceding publication,[5] the static magnetic field was obtained by evaluating Ampère's circuital law,

$$\nabla \times \mathbf{H} = \mathbf{J}, \tag{2}$$

for a vacuum filled vessel confined by an electric coil. The magnetic induction inside the vessel then is given by $\mathbf{B} = \mu_0 \mathbf{H}$. If the permeability can be considered homogeneous, the law of Biot-Savart,

$$\mathbf{B}(\mathbf{x}) = \frac{\mu_0}{4\pi} \int \mathbf{J}(\mathbf{x}') \times \frac{\mathbf{x} - \mathbf{x}'}{|\mathbf{x} - \mathbf{x}'|^3}\, \mathrm{d}^3 x', \tag{3}$$

offers a valid solution for the magnetic induction for arbitrary coil geometries.[6] An algorithmic version of this law was developed to determine the magnetic induction within an adjustable simulation domain.

To be able to calculate induced electric fields based on Faraday's law, the magnetostatic fields can be taken as basis for further investigations. The law of Biot-Savart is still valid in the quasi-stationary regime because **J** can be assumed to be constant and thus can also be used to calculate the magnetic induction for radio-frequency currents through short electrical coils. In this regime, retardation effects are not taken into account which explains that some magnetostatic relations are still valid. One of those relations is the Vector Poisson equation,

$$\nabla^2 \mathbf{A} = -\mu_0 \mathbf{J}, \tag{4}$$

in this case, for non-magnetic materials satisfying $\mu = \mu_0$. Its derivation can be seen elsewhere.[6] A possible solution for this partial differential equation of elliptic type is given by

$$\mathbf{A}(\mathbf{x}) = \frac{\mu_0}{4\pi} \int \frac{\mathbf{J}(\mathbf{x}')}{|\mathbf{x} - \mathbf{x}'|} \, \mathrm{d}^3 x' \tag{5}$$

which can be used to obtain the vector potential.

The second Maxwell equation states that there are no magnetic monopoles; i.e,

$$\nabla \cdot \mathbf{B} = 0, \tag{6}$$

thus that **B** has to be the curl of another vector field; i.e., the vector potential **A**.[6] The mathematical definition reads as follows:

$$\mathbf{B} = \nabla \times \mathbf{A} \tag{7}$$

If Eq. (5) is substituted into Eq. (7) the law of Biot-Savart (Eq. (3)) is obtained. This relation is useful for coupling the vector potential to the electric field (that should be computed) which will be shown in the following.

With Eq. (7) being substituted into Faraday's law (Eq. (1)), the following relation is obtained:

$$\nabla \times \mathbf{E} + \frac{\partial}{\partial t} (\nabla \times \mathbf{A}) = 0 \tag{8}$$

Using Schwarz's integrability condition,[8] the partial differentials can be rearranged as follows:

$$\nabla \times \mathbf{E} + \nabla \times \frac{\partial \mathbf{A}}{\partial t} = \nabla \times \left(\mathbf{E} + \frac{\partial \mathbf{A}}{\partial t} \right) = 0 \tag{9}$$

As the curl of the parenthesized expression vanishes, it can be regarded as the gradient of a scalar potential Φ.[6,8] After rearrangement, an expression for the electric field can be given by

$$\mathbf{E} = -\nabla \Phi - \frac{\partial \mathbf{A}}{\partial t}. \tag{10}$$

This combination of scalar and vector potential is often referred to as "electrodynamic potential".

B. Numerical Solution

As the electric field inside an evacuated vessel should be obtained, we assume that no free charges are present within the whole simulation domain. This will lead to a vanishing scalar potential and thereby a manipulation of Eq. (10), resulting in:

$$\mathbf{E} = -\frac{\partial \mathbf{A}}{\partial t} \tag{11}$$

The first approach is to obtain the spatially varying vector potential. As already mentioned, the quasi-stationary constraint dictates that the current through the coil needs to be homogeneous. For better transparency between simulation and measurement, an impedance model of the coil is introduced which determines the amount of current drawn from a generator.

Using radio-frequencies, the skin effect inevitably needs to be taken into account. The skin depth is given by

$$\delta = \sqrt{\frac{2}{\sigma \omega \mu}}, \tag{12}$$

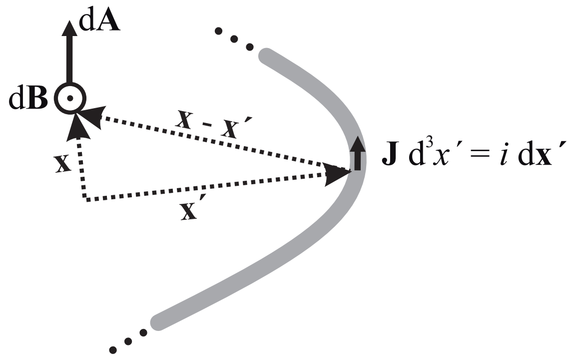

Figure 1. Vectors within the simulation domain.

where $\mu = \mu_0 \mu_r$. The skin effect decreases the effective area A_{eff} the current runs through, causing the coil wire resistance to increase.[6] The equivalent DC resistance of any conductor is given by

$$R_{\text{DC}} = \frac{l}{\sigma A_{\text{eff}}}. \tag{13}$$

Since the solver offers handling of arbitrarily shaped coil geometries, the length of each coil can be determined numerically. Therefore, the coil is discretized into several elements. As can be seen in Fig. 1, the vector $\mathbf{x}'$ points to one coil element at a time. The length of one coil element then calculates to (assuming the coil is equally discretized):

$$\mathrm{d}\mathbf{x}' = \lim_{\mathbf{x}'_k \to 0} \left(\mathbf{x}'_{k+1} - \mathbf{x}'_k\right) \approx \Delta\mathbf{x}' = \mathbf{x}'_{k+1} - \mathbf{x}'_k \tag{14}$$

To obtain the total length, those discrete coil elements are summed up in a loop:

$$l = \sum_k \left(\mathbf{x}'_{k+1} - \mathbf{x}'_k\right) \tag{15}$$

Once the length is obtained, Eq. (13) can be computed for different coil diameters and materials. Together with the formerly obtained inductance of the coil,[5] its impedance then calculates to

$$Z = R_{\text{DC}} + \mathrm{i}\omega L, \tag{16}$$

where the parasitic parallel capacitance is neglected due to the low radio-frequency applied. If a rf voltage (e.g. $v(t) = \hat{v}\cos(\mathrm{i}\omega t)$) is applied to the coil, the current is determined by its impedance:

$$i(t) = \Re\left\{\frac{\hat{v}}{|Z|}\exp\left[\mathrm{i}\omega t - \arctan\left(\frac{\omega L}{R_{\text{DC}}}\right)\right]\right\} \tag{17}$$

Since the current through the coil can now be calculated, Eq. (5) may be computed. Using the constraints of the quasi-stationary regime, the current can be assumed homogeneous and thus does not have to be evaluated in the integral. This leads to a simplified form of Eq. (5) given by

$$\mathbf{A}(\mathbf{x}, t) = \frac{\mu_0 i(t)}{4\pi} \int \frac{\mathrm{d}\mathbf{x}'}{|\mathbf{x} - \mathbf{x}'|}. \tag{18}$$

The time dependent current at $\mathbf{x}'$ generates an infinitesimal contribution to the vector potential (and thus to the magnetic induction which is described in the following) at $\mathbf{x}$ (cf. Fig. 1). The numerical form of Eq. (18) can now easily be derived:

$$\mathbf{A}(\mathbf{x}_j, t) = \frac{\mu_0 i(t)}{4\pi} \sum_k \frac{\Delta\mathbf{x}'}{|\mathbf{x}_j - \mathbf{x}'_k|} \tag{19}$$

This algorithm can be computed using nested loops or matrix operations.

With knowledge of the spatially and temporally varying vector potential, the corresponding magnetic induction as well as the electric field can be determined using Eqs. (7) and (11). The curl of the vector potential at $\mathbf{x}_j$ in Cartesian space can be calculated as

$$\begin{aligned}\mathbf{B}\left(\mathbf{x}_j,t\right) = &\left(\frac{A_{x_3}\left(\mathbf{x}_{j+1},t\right)-A_{x_3}\left(\mathbf{x}_j,t\right)}{x_2\left(\mathbf{x}_{j+1}\right)-x_2\left(\mathbf{x}_j\right)}-\frac{A_{x_2}\left(\mathbf{x}_{j+1},t\right)-A_{x_2}\left(\mathbf{x}_j,t\right)}{x_3\left(\mathbf{x}_{j+1}\right)-x_3\left(\mathbf{x}_j\right)}\right)\mathbf{u}_{x_1}\\ &+\left(\frac{A_{x_1}\left(\mathbf{x}_{j+1},t\right)-A_{x_1}\left(\mathbf{x}_j,t\right)}{x_3\left(\mathbf{x}_{j+1}\right)-x_3\left(\mathbf{x}_j\right)}-\frac{A_{x_3}\left(\mathbf{x}_{j+1},t\right)-A_{x_3}\left(\mathbf{x}_j,t\right)}{x_1\left(\mathbf{x}_{j+1}\right)-x_1\left(\mathbf{x}_j\right)}\right)\mathbf{u}_{x_2}\\ &+\left(\frac{A_{x_2}\left(\mathbf{x}_{j+1},t\right)-A_{x_2}\left(\mathbf{x}_j,t\right)}{x_1\left(\mathbf{x}_{j+1}\right)-x_1\left(\mathbf{x}_j\right)}-\frac{A_{x_1}\left(\mathbf{x}_{j+1},t\right)-A_{x_1}\left(\mathbf{x}_j,t\right)}{x_2\left(\mathbf{x}_{j+1}\right)-x_2\left(\mathbf{x}_j\right)}\right)\mathbf{u}_{x_3},\end{aligned} \tag{20}$$

with $\mathbf{x} = x_1\mathbf{u}_{x_1} + x_2\mathbf{u}_{x_2} + x_3\mathbf{u}_{x_3}$. Furthermore, the electric field in that point calculates to

$$\mathbf{E}\left(\mathbf{x}_j,t_i\right) = -\frac{\mathbf{A}\left(\mathbf{x}_j,t_{i+1}\right)-\mathbf{A}\left(\mathbf{x}_j,t_i\right)}{t_{i+1}-t_i}. \tag{21}$$

In the next section, simulation results for the electric field and magnetic induction, respectively, are presented.

III. Simulation Results

The simulated short solenoidal coil has a radius of 25 mm, an axial length of 40 mm, and 8 windings, as can be seen in Fig. 2 (a).

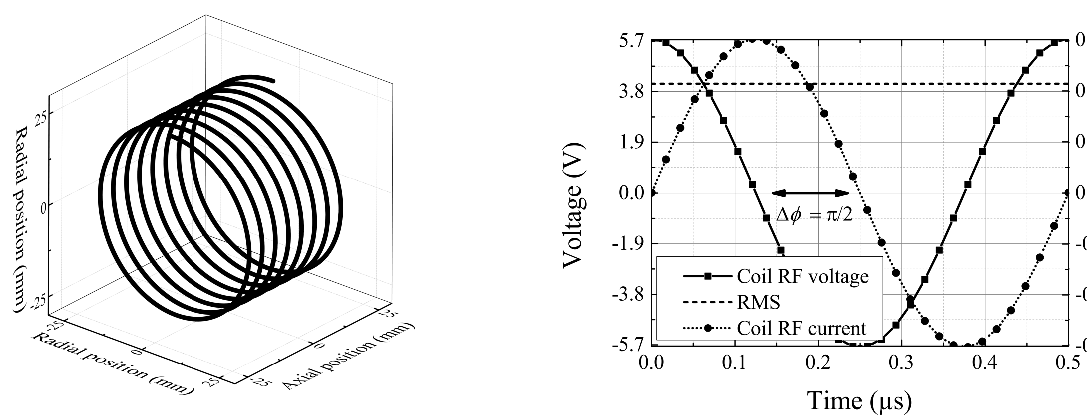

(a) (b)

Figure 2. (a) Short solenoidal geometry in simulation domain. (b) Voltage and current applied to the coil.

A 2 MHz rf voltage with $\hat{v} = 5.69\,\mathrm{V}$ is applied to the coil. With an impedance of $(0.063 + \mathrm{i}\,31.32)\ \Omega$ (cf. Eq. (16)), the resulting current can be seen in Fig. 2 (b). The simulated 3-dimensional magnetic induction and electric field vectors are depicted in Figs. 3 (a) and (b), respectively.

To obtain a better understanding of the magnitudes of the vector fields, Figs. 4 (a) and (b) show surface plots of the magnetic induction field strength (B) in axial and radial direction (a) and the electric field strength (E) in radial direction (b). Each plot is evaluated on the corresponding cut-plane through the coil.

The direction of the vectors together with their magnitude on each plane is depicted in Figs. 5 (a) and (b), respectively. These figures show that the magnetic induction vectors are non-uniformly distributed within the coil. This is the reason why the induced magnetic field of coils with such geometries (e.g. short solenoidal) has to be evaluated numerically. There is often no closed solution that can be described analytically.[6,7]

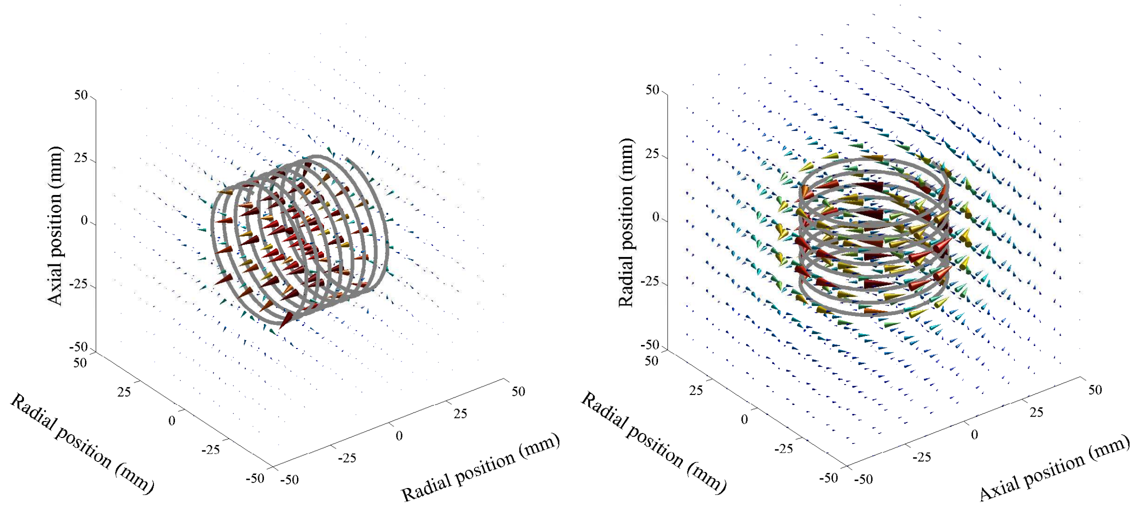

(a) (b)

Figure 3. (a) Magnetic induction vectors. (b) Electric field vectors.

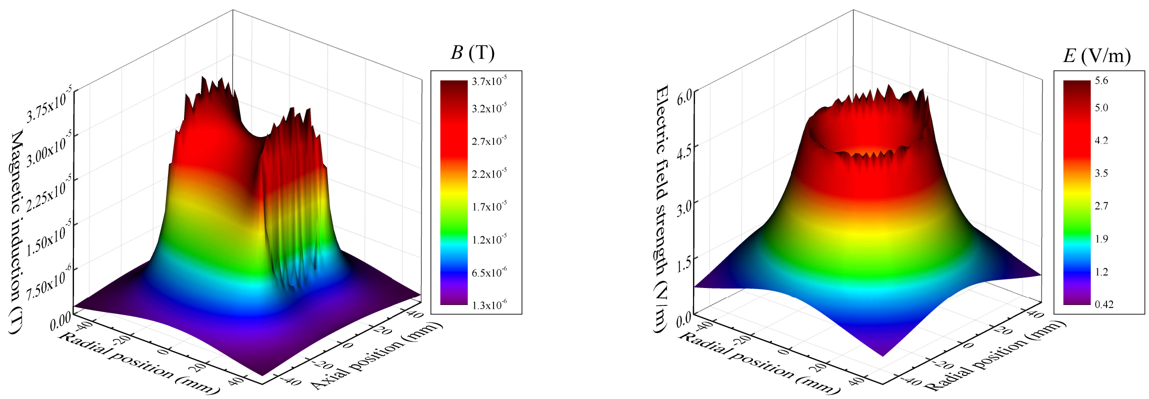

(a) (b)

Figure 4. (a) Magnetic induction field strength on axial cut-plane. (b) Electric field strength on radial cut-plane.

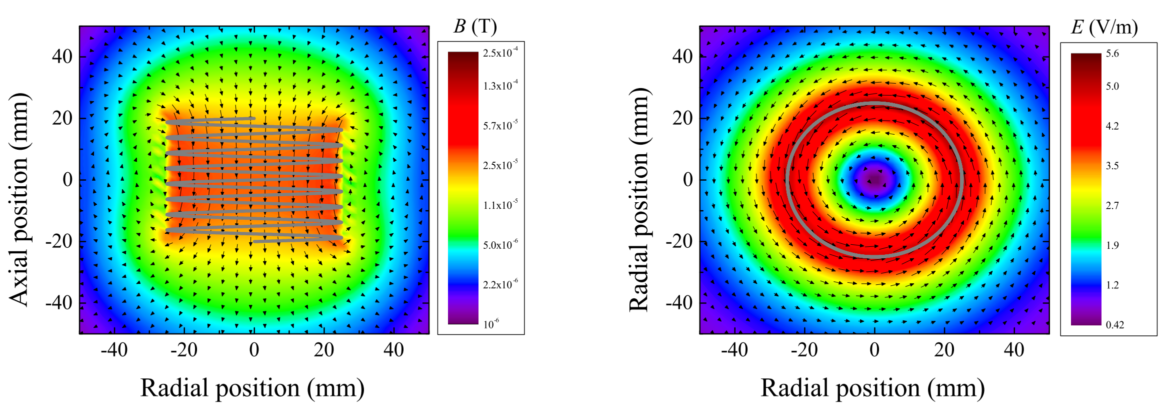

(a) (b)

Figure 5. (a) Magnetic induction field vectors on axial cut-plane. (b) Electric field vectors on radial cut-plane.

IV. Verification by Measurement

The verification of the magnetic induction based on the coil's inductance is described in another publication.[5] Here, we want to verify the electric field inside the coil that is generated by the time-varying magnetic induction. For the measurement, a generic field probe based on a coaxial cable was assembled, as can be seen in Fig. 6. Its circular antenna with radius of 14 mm follows the shape of the electric field vectors and is so intended to catch exactly one circularly induced voltage path inside the coil. The coil which is wound around a vessel is depicted in Fig. 7. Due to the tangential boundary condition;[6,7] i.e., $E_{\mathrm{t1}} = E_{\mathrm{t2}}$, the permittivity of the vessel does not change the circularly induced electric field strength at the boundary between vessel and vacuum. Any normal components are neglected because of the circular form of the electric field.

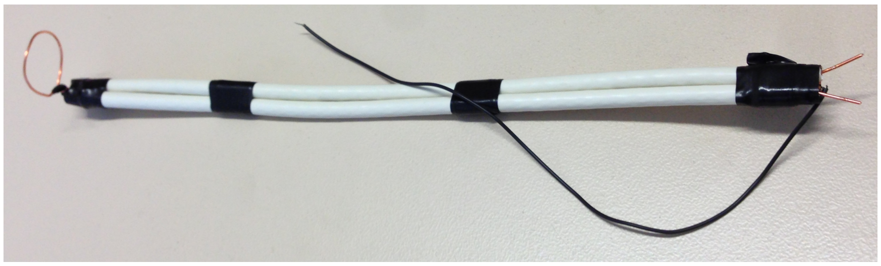

Figure 6. Generic electric field probe.

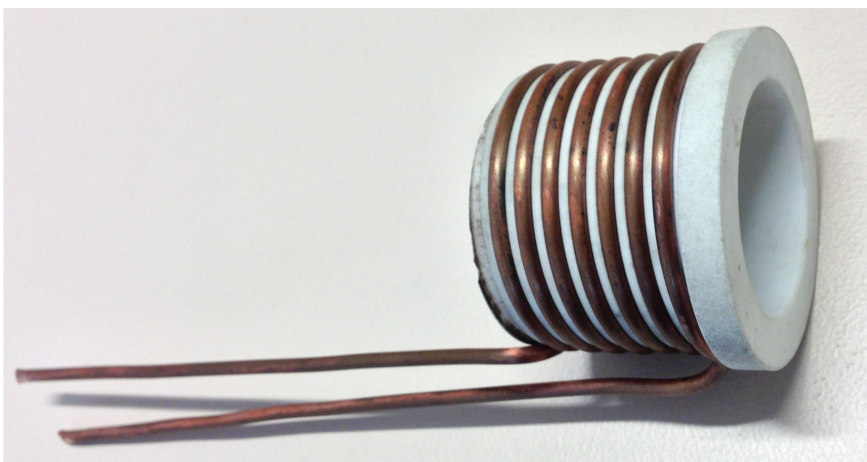

Figure 7. Coil and discharge vessel.

The field strength was measured at four axial points and the measurement values are shown in Fig. 8. The simulated data are also shown in this figure and show a quite good agreement to the measurement; although the generic probe was never calibrated.

V. Conclusion and Outlook

In this paper, we presented a numerical solution of Faraday's law of induction for arbitrary coil geometries; i.e., current paths. The solver was verified by measurements conducted with a generic electric field probe and the results agree well.

This solver is the basis for a model of an inductively-coupled plasma generator, as used in radio-frequency ion thrusters. The future work will consist of the incorporation of free charge carriers that cause a scalar potential within the simulation domain. Therefore, the existing model has to be revised, since the electric field depends not only on the vector potential that varies with time but also on the scalar potential. The latter potential again depends on the fields obtained in this work and additionally, it will superpose the existing potential, hence an iterative solution for the fields has to be modeled.

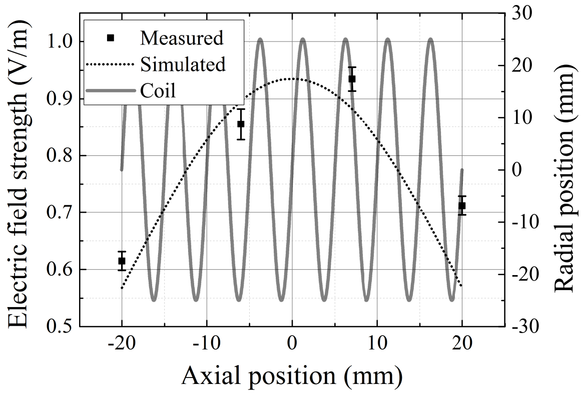

Figure 8. Verification of the solver.

The ICP model is supposed to yield the electric characteristics of the plasma generator, consisting of coil and plasma.[1,9,10] The electric parameters are needed to describe the plasma as an equivalent circuit for engineering purposes like the design of matching networks and control loops.

VI. Acknowledgment

We would like to thank Peter J. Klar and Bruno Meyer from the Giessen University for their cooperation. This project is funded by the Hessian State Ministry of Higher Education, Research and the Arts within the LOEWE-project RITSAT.

References

[1] Liebermann, M. A., and Lichtenberg, A. J., *Principles of Plasma Discharges and Materials Processing*, 2nd ed., John Wiley & Sons, New Jersey, 2005.

[2] Ley, W., Wittman, K., and Hallmann, W., *Handbook of Space Technology*, AIAA, 2009.

[3] Goebel, D. M., and Katz, I., *Fundamentals of Electric Propulsion: Ion and Hall Thrusters (JPL Space Science and Technology Series)*, Wiley, 2008.

[4] Loeb, H. W., "Radio Frequency Ion Sources for Electrostatic Propulsion (Hollow Cathode Design for Electron Bombardment Radio Frequency Ion Thruster Source)", *Proceedings of the Symposium on Ion Sources and Formation of Ion Beams*, pp. 77-84, 1971.

[5] Volkmar, C., Baruth, T., Simon, J., Ricklefs, U., and Thueringer, R., "Arbitrarily Shaped Coils' Inductance Simulation Based on a 3-Dimensional Solution of the Biot-Savart Law", *Proceedings of the 36th International Spring Seminar on Electronics Technology*, submitted for publication, 2013.

[6] Jackson, J. D., *Classical Electrodynamics*, 3rd ed., Wiley, 1998.

[7] Purcell, E. *Electricity and Magnetism*, 2nd ed., Cambridge University Press, 2011.

[8] Bronshtein, I. N., Semendyayev, K. A., Musiol, G., and Muehlig, H., *Handbook of Mathematics*, 5th ed., Springer, 2007.

[9] Chabert, P., and Braithwaite, N., *Physics of Radio-Frequency Plasmas*, Cambridge University Press, 2011.

[10] Chen, F. F., *Introduction to Plasma Physics and Controlled Fusion*, corr. 2nd ed., Springer, 2006.